A&A 545, A74 (2012)
DOI: 10.1051/0004-6361/201219151

Astronomy & Astrophysics

Detection of diffuse radio emission in the galaxy clusters A800, A910, A1550, and CL 1446+26

F. Govoni[1], C. Ferrari[2], L. Feretti[3], V. Vacca[1,4], M. Murgia[1], G. Giovannini[3,5], R. Perley[6], and C. Benoist[2]

[1] INAF – Osservatorio Astronomico di Cagliari, Strada 54, Loc. Poggio dei Pini, 09012 Capoterra (Ca), Italy
e-mail: fgovoni@ira.inaf.it
[2] Laboratoire Lagrange, UMR7293, Université de Nice Sophia-Antipolis, CNRS, Observatoire de la Côte d'Azur, 06300 Nice, France
[3] INAF – Istituto di Radioastronomia, via P. Gobetti 101, 40129 Bologna, Italy
[4] Dipartimento di Fisica, Università degli Studi di Cagliari, Cittadella Universitaria, 09042 Monserrato (CA), Italy
[5] Dipartimento di Astronomia, Università degli Studi di Bologna, via Ranzani 1, 40127 Bologna, Italy
[6] National Radio Astronomy Observatory, Socorro, NM 87801, USA

Received 2 March 2012 / Accepted 10 July 2012

ABSTRACT

Context. Radio halos are elusive sources located at the center of merging galaxy clusters. To date, only about 40 radio halos are known, thus the discovery of new halos provides important insights into this class of sources.
Aims. To improve the quality of the statistics of radio halos, we investigate the radio continuum emission of a sample of galaxy clusters.
Methods. We analyzed archival Very Large Array observations at 1.4 GHz, with a resolution of $\simeq 1'$. These observations were complemented by X-ray, optical, and higher-resolution radio data, leading to the detection of a new radio halo in the central region of A800 and A1550. We discovered a radio relic in the periphery of A910, and finally revealed both a halo and a relic in CL1446+26.
Results. The clusters hosting these new halos show an offset between the radio and the X-ray peak. By analyzing this offset statistically, we find that radio halos can be quite asymmetric with respect to the X-ray gas distribution, with an average radio-X-ray displacement of about 180 kpc. When the offsets are normalized by the halo size, there is a tendency for smaller halos to have larger displacements.

Key words. galaxies: clusters: general – large-scale structure of Universe – magnetic fields

1. Introduction

Sensitive radio observations have revealed diffuse emission from the central regions of some merging galaxy clusters (e.g. Giovannini et al. 1999; Giovannini & Feretti 2000; Kempner & Sarazin 2001; Govoni et al. 2001a; Bacchi et al. 2003; Venturi et al. 2007; Venturi et al. 2008; van Weeren et al. 2009; Rudnick & Lemmerman 2009; Giovannini et al. 2009; van Weeren et al. 2011). These radio sources, which extend over volumes of $\sim$1 Mpc^3 and are called radio halos, are diffuse, low-surface-brightness ($\simeq 1\ \mu$Jy arcsec^{-2} at 1.4 GHz), and steep-spectrum[1] ($\alpha > 1$) synchrotron sources with no obvious optical counterparts (see e.g. Ferrari et al. 2008; Feretti et al. 2012).

Radio halos can have quite different length-scales, but the largest halos are the most powerful, in such a way that all these sources may have similar synchrotron emissivities (Murgia et al. 2009). Their radio power at 1.4 GHz correlates with the cluster X-ray luminosity (Feretti 2002), temperature (Liang 1999; Colafrancesco 1999), mass (Govoni et al. 2001a), and Sunyaev-Zel'dovich effect (Basu 2012) measurements.

The radio halo morphology is often very similar to the X-ray-emitting thermal intracluster medium (e.g. Govoni et al. 2001b; Feretti et al. 2001; Keshet & Loeb 2010; Brown & Rudnick 2011). Furthermore, radio halos are preferentially found in clusters that show evidence of merger activity (e.g. Buote 2001; Schuecker et al. 2001; Govoni et al. 2004; Cassano et al. 2010; Rossetti et al. 2011), which suggests a connection between the origin of radio halos and the gravitational processes of cluster formation, although a one-to-one association between merging clusters and radio halos is not supported by present observations.

Detailed images of radio halos can provide information on the cluster magnetic field, since the halo brightness fluctuations and the polarization level are strictly related to the intracluster magnetic field power spectrum (Tribble 1991; Murgia et al. 2004; Govoni et al. 2006). Vacca et al. (2010) presented a study of the magnetic field power spectrum in the galaxy cluster A665, which contains a Mpc-scale radio halo. Their modeling suggests that radio halos can be effectively polarized, but because of their faintness, detecting this polarized signal is a very hard task with the current radio interferometers. Radio halos are indeed usually found to be unpolarized. Polarized emission from radio halos has been observed so far only in the filaments of the clusters A2255 (Govoni et al. 2005; see also Pizzo et al. 2011) and MACS J0717+3745 (Bonafede et al. 2009).

The statistics of radio halos remain poor because of their faintness. To date, only about 40 radio halos are known (see e.g. the compilation of Feretti et al. 2012, and references therein), thus the discovery of new halos provides important insights into this class of sources. As part of an ongoing program to investigate, in complex X-ray cluster systems, the presence of halo emission from the sub-clusters in the merger, we recently discovered the case of the double merging system, A399 and A401, which both contain a radio halo and can be considered the only case so far of a double-radio halo system (Murgia et al. 2010). We also detected an intriguing case of diffuse radio emission

[1] $S(\nu) \propto \nu^{-\alpha}$, with α = spectral index.

Table 1. Details of the VLA observations.

Cluster	RA (J2000)	Dec (J2000)	Frequency (GHz)	Bandwidth (MHz)	Conf.	Obs. time (min)	Date	Program
A800	09 28 22.9	37 48 09.0	1365/1435	7×3.125	D	15	1995-March-15	AM0469
	09 25 41.9	37 56 50.0	1452/1502	25	C	7	1984-May-04	AO0048
A910	10 02 57.7	67 09 23.0	1365/1435	7×3.125	D	15	1995-March-15	AM0469
	10 03 18.8	67 11 02.4	1465/1385	50	C	3	1993-Jun-28	AL0297
A1550	12 29 19.2	47 37 58.0	1365/1435	7×3.125	D	15	1995-March-15	AM0469
	12 28 57.7	47 37 58.0	1365/1435	7×3.125	C	75	2003-Jan-03	AM0702
CL1446+26	14 49 28.7	26 07 54.1	1365/1435	7×3.125	D	20	1995-March-15	AM0469

Notes. Column 1: cluster name; Cols. 2, 3: observation pointing (RA J2000, Dec J2000); Col. 4: frequency (IF1/IF2); Col. 5: bandwidth; Col. 6: VLA configuration; Col. 7: observing time (minutes); Col. 8: observing date; Col. 9: VLA program.

in A781 (Govoni et al. 2011), which is an exceptional system characterized by a complex of several clusters. The archival VLA data set containing the observation of A781 includes uniform observations for several galaxy clusters. Thus, to improve the scanty statistics of radio halos, we analyzed the entire data set and the results of this investigation, complemented by X-ray, optical, and higher-resolution radio data, are presented in this work.

The intrinsic parameters quoted in this paper are computed for a ΛCDM cosmology with $H_0 = 71\ \mathrm{km\,s^{-1}\,Mpc^{-1}}$, $\Omega_\mathrm{m} = 0.27$, and $\Omega_\Lambda = 0.73$. Values taken from the literature have been scaled to this cosmology.

2. VLA observations and data reduction

We analyzed archival observations taken with the VLA at 1.4 GHz in D configuration (VLA program AM0469). This data set contains 41 galaxy clusters observed on average for 15 min each. A brief discussion of the quality of these data is given in the appendix.

The data were calibrated in phase and amplitude. Data editing was made in order to excise RFI. Since the observations had been done in spectral line mode, data were calibrated in bandpass and data editing was made channel by channel. Surface brightness images were produced following the standard procedures of Fourier-Transform, Clean, and Restore implemented in the AIPS task IMAGR. We used the multi-scale Clean (see e.g. Greisen et al. 2009), which is an extension of the classical Clean algorithm, implemented in the task IMAGR. We averaged the two IFs (and the seven channels) together in the gridding process under IMAGR. Self-calibration (phase) was performed to increase the dynamic range and the sensitivity of the radio images. The spectral line mode of this data set is unsuitable for producing polarization-sensitive images.

We detected evidence of diffuse radio emission in seven clusters already known to host a radio halo: A1758, A851, A1995 (Giovannini et al. 2009); A1351 (Giacintucci et al. 2009; Giovannini et al. 2009); A773, A2254 (Govoni et al. 2001a); and A2219 (Bacchi et al. 2003; Orrú et al. 2007).

In addition, we discovered new diffuse sources in A800, A910, A1550, CL1446+26, and A781. We analyzed the radio continuum emission and the spectral index properties between 1.4 GHz and 0.3 GHz of A781 in a separate paper (Govoni et al. 2011). In this paper, we present the properties of the remaining four clusters (A800, A910, A1550, CL1446+26), for which only data at 1.4 GHz are available in the archive. We note that a peripheral diffuse emission, classified as a radio relic, was previously detected in CL1446+26 by Giovannini et al. (2009).

Table 2. Information on discrete radio sources.

Cluster	Label	RA (J2000)	Dec (J2000)	$S_{1.4\ \mathrm{GHz}}$ (mJy)
A800	A	09 28 36.1	37 47 06	3.5 ± 0.3
	B	09 28 27.5	37 45 12	2.3 ± 0.2
A910	A	10 03 20.8	67 09 32	25.2 ± 1.3
	B	10 03 15.2	67 10 20	4.9 ± 0.3
	C	10 03 14.1	67 11 09	1.8 ± 0.2
	D	10 03 15.3	67 12 00	0.7 ± 0.2
	E	10 03 24.7	67 13 22	2.8 ± 0.3
	F	10 03 32.2	67 11 20	2.8 ± 0.3
A1550	A	12 29 02.3	47 36 56	15.8 ± 0.8
	B	12 28 58.5	47 38 26	2.2 ± 0.2
	C	12 29 15.7	47 37 04	0.8 ± 0.2
CL1446+26	A	14 49 29.7	26 07 54	29.7 ± 1.5
	B	14 49 28.2	26 08 22	2.4 ± 0.2
	C	14 49 30.6	26 09 11	2.2 ± 0.2
	D	14 49 33.1	26 04 06	11.0 ± 0.5
	E	14 49 26.7	26 05 21	3.2 ± 0.2
	F	14 49 18.2	26 05 30	2.5 ± 0.2

Notes. Column 1: cluster name; Col. 2: source label; Cols. 3, 4: source position (RA J2000, Dec J2000); Col. 5: source flux density (from the C array data set).

However, on the basis of the data presented here the classification of the diffuse emission in this cluster is more complex than previously stated.

The details of the analyzed radio observations (pointing, frequency, bandwidth, VLA configuration, observing time, observing date, and VLA program) are reported in Table 1.

To separate the diffuse radio emission from discrete sources, we produced with standard procedures images at higher resolution obtained at 1.4 GHz with the VLA in C configuration for the galaxy clusters A800, A910, and A1550. In the case of CL1446+26, we used the VLA data in C configuration previously analyzed by Giovannini et al. (2009).

The position and the flux density[2] of the discrete sources embedded in the cluster diffuse emission are given in Table 2. These values were subtracted from the flux density obtained by integrating the surface brightness of the D array data set down to the 3σ level to estimate the residual flux density of the diffuse emission (see Table 3). We note, however, that the residual flux density associated with the diffuse cluster emission must be interpreted with caution. A possible variation in the flux density of discrete sources, the slightly different frequency of the two data

[2] All the flux densities given in the tables and in the text have been primary-beam-corrected.

Table 3. Radio information of clusters containing diffuse emission.

Name	z	kpc/″	Type	$S_{1.4\,\mathrm{GHz}}$ (mJy)	log $P_{1.4\,\mathrm{GHz}}$ (W/Hz)	LLS (Mpc)	Radio-X-ray Offset (″)	Radio-optical Offset (″)
A800	0.2223	3.55	H	10.6	1.52×10^{24}	1.28	90	5
A910	0.2055	3.34	R	12.1	1.45×10^{24}	1.00	135	200
A1550	0.2540	3.92	H	7.7	1.49×10^{24}	1.41	105	5
CL1446+26N	0.370	5.09	H	7.7	3.57×10^{24}	1.22	85	40
CL1446+26S	0.370	5.09	R	5.3	2.46×10^{24}	1.53	205	250

Notes. Column 1: cluster name; Col. 2: redshift; Col. 3: angular-to-linear conversion; Col. 4: type of diffuse radio emission: H = halo, R = relic; Col. 5: diffuse radio flux density at 1.4 GHz; Col. 6: diffuse radio power at 1.4 GHz; Col. 7: radio largest linear size (LLS); Col. 8: radio-X-ray offset; Col. 9: radio-optical offset.

sets, and any absolute calibration error between them could result in an under-subtraction or over-subtraction of the calculated flux density. In addition, owing to the short exposure time of the archival observations, some diffuse emission could be missed. Therefore, a deep follow-up investigation would be necessary to ensure the recovery of the entire radio flux and unambiguously separate the diffuse emission from that of the unrelated discrete sources.

To ascertain that the large-scale diffuse emission is not caused by the blending of discrete sources, for each cluster we obtained a total intensity image at 1.4 GHz with the VLA in D configuration, after subtraction of discrete sources. We first produced an image of the discrete sources by using only the longest baselines of the D configuration data set. The clean components of the discrete sources were then subtracted from the original data set in the uv-plane by using the AIPS task UVSUB. At this point, we calculated the flux density of the residual diffuse emission by integrating the surface brightness down to the 3σ level, and we checked its consistency with the values reported in Table 3. We found that the agreement is generally good (see the notes on individuals clusters).

3. New detections of diffuse radio emission

For each cluster, we analyze the results of the VLA observations with a particular emphasis on the analysis of the radio properties of the large-scale cluster diffuse emission.

There are only sparse radio, X-ray, and optical information in the literature for the clusters analyzed in this paper, and nothing is reported about their dynamical state. To test the possible connection between the detection of diffuse radio emission and the dynamical state of the observed clusters, we compare our results with the gas and galaxy distributions of each system.

We investigated the gaseous environments of these clusters by checking their X-ray emission in the Rosat All Sky Survey (RASS). The X-ray images in the 0.1−2.4 keV band were background-corrected, exposure-corrected, and smoothed with a $\sigma = 45''$ Gaussian kernel.

We produced density maps of the bi-dimensional galaxy distribution of each observed cluster on the basis of a multi-scale approach, as described in Ferrari et al. (2005). To avoid projection effects as much as possible, we selected galaxies lying on the cluster red-sequence and brighter than $L^* + 3$. For most of the systems of our sample, we used the Sloan Digital Sky Survey (SDSS) multi-band galaxy catalog (Abazajian et al. 2009), applying a color–magnitude selection based on the $(r - i)$ vs. r and $(i - z)$ vs. r plots (see, e.g., Goto et al. 2002). Only the field around A910 is not covered by SDSS observations, therefore we exploited the SuperCOSMOS catalog (Hambly et al. 2001) and used the $(B - R)$ vs. B and $(B - R)$ vs. R plots for color selection.

In the following, for each cluster we compare the radio emission with optical and X-ray images.

3.1. Abell 800

A800 (RXCJ0928.6+3747) is a low X-ray luminosity cluster at a redshift $z = 0.2223$, which is part of the Northern ROSAT All-Sky (NORAS) Galaxy Cluster Survey by Böhringer et al. (2000). Its X-ray luminosity in the 0.1−2.4 keV band is 2.25×10^{44} erg/s.

Low resolution radio contours at 1.4 GHz of A800 are shown in the top-left and bottom-left panels of Fig. 1. This image was obtained with the VLA in D configuration and has been convolved to a resolution of $63'' \times 63''$. In the top panel, the radio contours are overlaid on the cluster X-ray image taken from the RASS. In the bottom panel, the radio contours are overlaid on the isodensity map of likely cluster members. The X-ray image shows an elongation in the northwest-southeast direction. The galaxy distribution has a main clump, surrounded by several substructures. The diffuse radio emission, which we classify as a radio halo, is concentrated within the main galaxy over densities, while a clear shift between the galaxies and gas distribution is present.

To separate the diffuse radio emission from discrete sources, we produced an image at higher resolution. In the bottom-right panel of Fig. 1, we present the radio contours of A800 at 1.4 GHz taken with the VLA in C configuration. This image has been convolved to a resolution of $17'' \times 17''$. The radio contours are overlaid on the optical image taken from the SDSS. Two discrete radio sources (labeled A and B) are embedded in the cluster diffuse emission. Source A is located south of the cluster X-ray center and coincides with the concentration of likely cluster members. Source B is located south-west of the cluster X-ray center at a projected distance of about 2.5′ from source A.

The total flux density is calculated from the D configuration image after a primary-beam correction by integrating the total surface-brightness intensity in the region of the diffuse emission down to the 3σ level. The resulting total flux density is estimated to be 16.4 ± 0.8 mJy. By subtracting the flux density (see Table 2) of the embedded discrete sources A and B, a flux density of 10.6 ± 0.9 mJy appears to be associated with the low-brightness diffuse emission. This flux density value corresponds to a radio power of $P_{1.4\,\mathrm{GHz}} = 1.52 \times 10^{24}$ W Hz^{-1}.

To ensure that the large-scale diffuse emission is not caused by the blending of discrete sources, in the top-right panel of Fig. 1 we present the total-intensity radio contours at 1.4 GHz with the VLA in D configuration after subtraction of discrete sources. In perfect agreement with the value given in Table 3, the flux density of the diffuse emission calculated in the image with the point sources subtracted is 10.7 ± 0.7 mJy. As measured

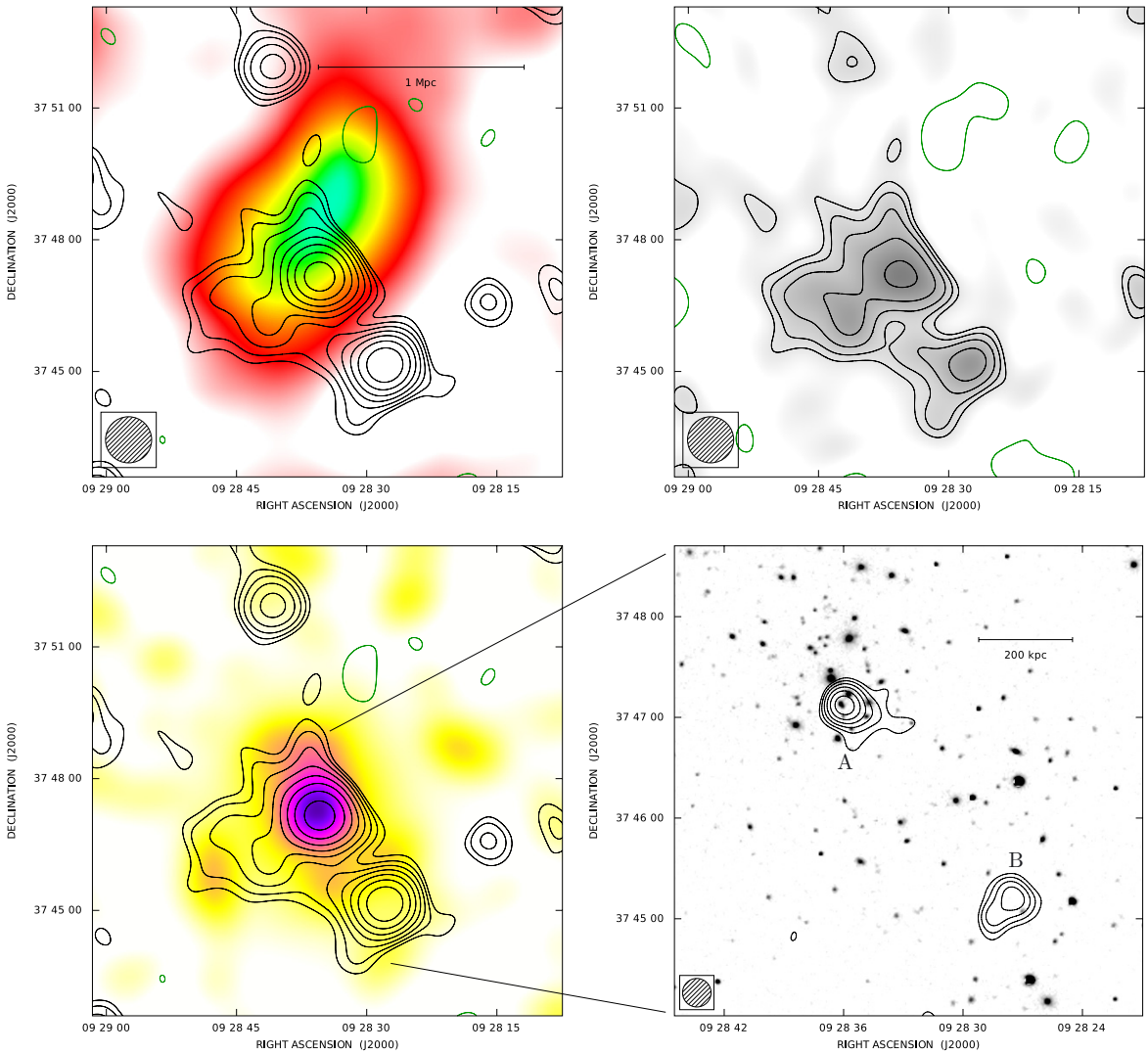

Fig. 1. Abell 800. *Top, left*: total intensity radio contours of A800 at 1.4 GHz with the VLA in D configuration. The image has a *FWHM* of $63'' \times 63''$. The contour levels are drawn at -0.35 (green), 0.35 mJy/beam, and the rest are spaced at intervals of a factor of $\sqrt{2}$. The sensitivity (1-σ) is 0.12 mJy/beam. Total intensity radio contours are overlaid on the Rosat PSPC X-ray image in the 0.1–2.4 keV band, taken from the RASS. The X-ray image has been convolved with a Gaussian of $\sigma = 45''$. *Top, right*: total intensity radio contours and grayscale image at 1.4 GHz with the VLA in D configuration after subtraction of discrete sources. *Bottom, left*: total intensity radio contours of A800 overlaid on the isodensity map of likely cluster members. *Bottom, right*: zoom of total intensity radio contours at the center of A800 at 1.4 GHz with the VLA in C configuration. The image has a *FWHM* of $17'' \times 17''$. The first contour level is drawn at 0.3 mJy/beam, and the rest are spaced at intervals of a factor of $\sqrt{2}$. The sensitivity (1σ) is 0.1 mJy/beam. The contours of the radio intensity are overlaid on the optical image taken from the SDSS (red plate).

from the 3σ radio isophote, the overall diffuse emission shows a largest linear size (LLS) of about $6'$ ($\simeq$1.28 Mpc). However, as pointed out in Murgia et al. (2009), we note that the size of the diffuse emission calculated from the contour levels should be carefully considered, since it depends on the sensitivity of the radio image.

3.2. Abell 910

A910 (RXCJ1003.1+6709) is a galaxy cluster at a redshift $z = 0.2055$ that belongs to the extended sample of the Rosat Brightest Cluster sample of Ebeling et al. (2000). Its X-ray luminosity in the 0.1–2.4 keV band is 3.32×10^{44} erg/s. This value agrees within the errors with that given by Böhringer et al. (2000).

The radio contours at 1.4 GHz of A910 are shown in the top-left and bottom-left panels of Fig. 2. This image was obtained with the VLA in D configuration and has been convolved to a resolution of $63'' \times 63''$. In the top panel, the radio contours are overlaid on the cluster X-ray image taken from the RASS. In the bottom panel, the radio contours are overlaid on the isodensity map of likely cluster members. In A910, at least three X-ray peaks can be identified, which are possible indications of a multiple merger. The galaxy distribution also shows several substructures. The diffuse radio emission is found to correspond to a bridge connecting a bright X-ray region with a fainter clump.

In the bottom-right panel of Fig. 2, we present the radio contours of A910 at 1.4 GHz taken with the VLA in C configuration. This image has been convolved to a resolution of $18'' \times 18''$. The radio contours are overlaid on the optical image taken from the Digital Sky Survey. Several discrete radio sources are embedded in the cluster diffuse emission.

We note that, in the classical framework of cluster radio-source classification (e.g. Ferrari et al. 2008; Feretti et al. 2012),

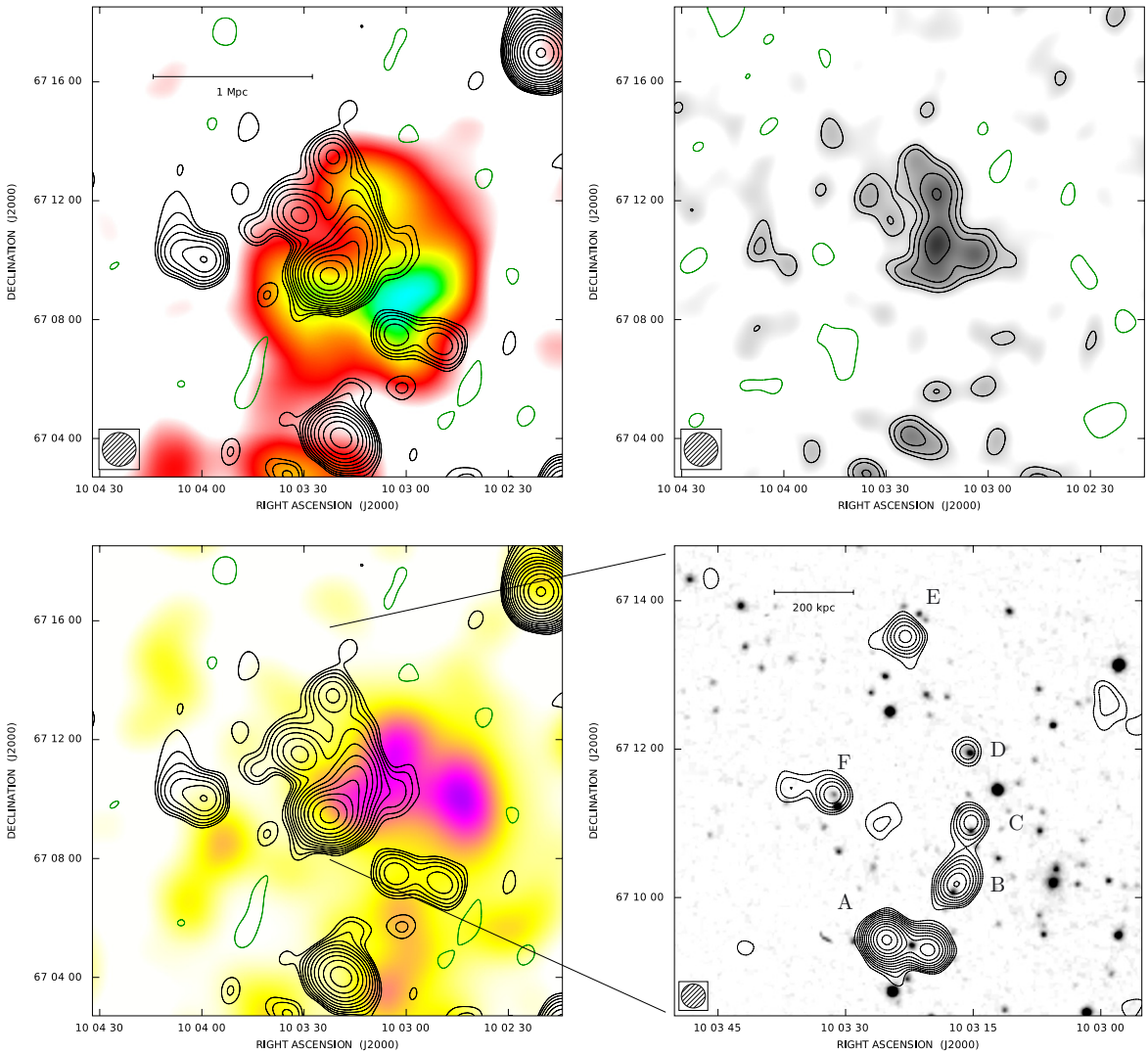

Fig. 2. Abell 910. *Top, left*: total intensity radio contours of A910 at 1.4 GHz with the VLA in D configuration. The image has a *FWHM* of $63'' \times 63''$. The contour levels are drawn at -0.45 (green), 0.45 mJy/beam, and the rest are spaced at intervals of a factor of $\sqrt{2}$. The sensitivity (1-σ) is 0.15 mJy/beam. Total intensity radio contours are overlaid on the Rosat PSPC X-ray image in the 0.1–2.4 keV band, taken from the RASS. The X-ray image has been convolved with a Gaussian of $\sigma = 45''$. *Top, right*: total intensity radio contours and grayscale image at 1.4 GHz with the VLA in D configuration after subtraction of discrete sources. *Bottom, left*: total intensity radio contours of A910 overlaid on the isodensity map of likely cluster members. *Bottom, right*: zoom of total intensity radio contours at the center of A910 at 1.4 GHz with the VLA in C configuration. The image has a *FWHM* of $18'' \times 18''$. The first contour level is drawn at 0.3 mJy/beam, and the rest are spaced at intervals of a factor of $\sqrt{2}$. The sensitivity (1σ) is 0.1 mJy/beam. The contours of the radio intensity are overlaid on the optical image taken from the Digital Sky Survey (red plate).

the diffuse radio source in A910 could be considered as a relic owing to its morphology and the offset between the radio and both the intracluster medium and the galaxy density peaks. As shown in top-right panel of Fig. 1 from which the discrete sources have been subtracted, the diffuse emission has an elongated structure with a LLS of about $5'$ ($\simeq$1.0 Mpc) that is offset from the main gas density and galaxy density peaks of about $135''$ (450 kpc) and about $200''$ (670 kpc), respectively. Therefore, given its location and morphology we classify this cluster diffuse emission as a relic.

The total flux density of the relic is calculated from the D configuration image by integrating the total intensity surface-brightness in the region of the diffuse emission down to the 3σ level. The resulting total flux density is estimated to be 50.3 ± 2.5 mJy. By subtracting the flux density of the discrete sources A, B, C, D, E, and F (see Table 2), a flux density of 12.1 ± 2.9 mJy appears to be associated with the low-brightness relic emission. This flux density value corresponds to a radio power of $P_{1.4\,\mathrm{GHz}} = 1.45 \times 10^{24}$ W Hz^{-1}. The flux density calculated in the image with the point sources subtracted is 9.0 ± 0.6 mJy, which is consistent within the errors with the value given above.

3.3. Abell 1550

A1550 (RXCJ1229.0+4737) is a galaxy cluster at a redshift $z = 0.2540$ with an X-ray luminosity in the 0.1–2.4 keV band of 3.51×10^{44} erg/s (Böhringer et al. 2000).

Low-resolution radio contours at 1.4 GHz of A1550 are shown in the top-left and bottom-left panels of Fig. 3. This image was obtained with the VLA in D configuration and has been convolved to a resolution of $53'' \times 53''$. In the top panel, the radio contours are overlaid on the cluster X-ray image taken from

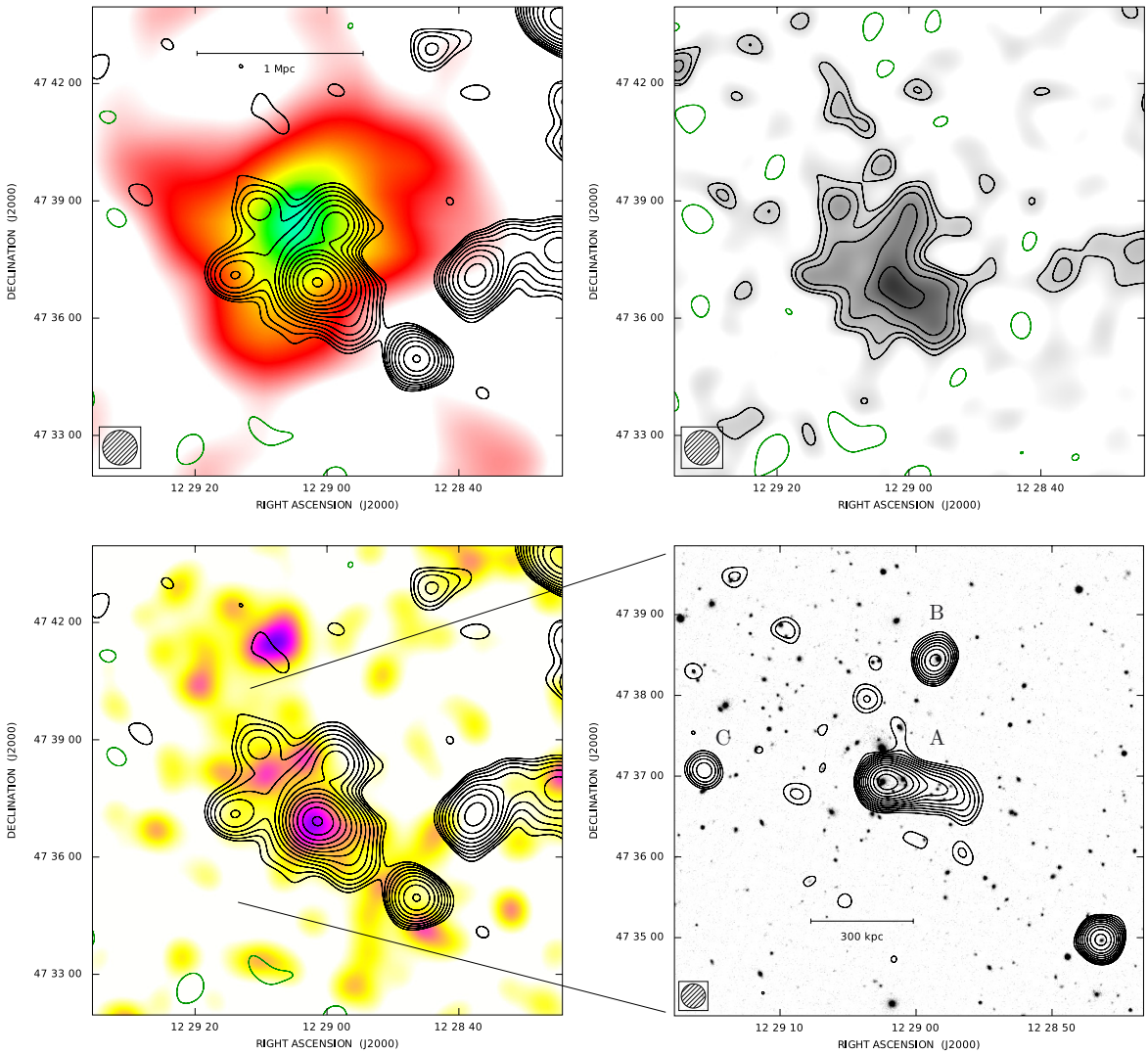

Fig. 3. Abell 1550. *Top, left*: total intensity radio contours of A1550 at 1.4 GHz with the VLA in D configuration. The image has a *FWHM* of $53'' \times 53''$. The contour levels are drawn at -0.2, 0.2 mJy/beam, and the rest are spaced at intervals of a factor of $\sqrt{2}$. The sensitivity (1-σ) is 0.07 mJy/beam. Total intensity radio contours are overlaid on the Rosat PSPC X-ray image in the 0.1–2.4 keV band, taken from the RASS. The X-ray image has been convolved with a Gaussian of $\sigma = 45''$. *Top, right*: total intensity radio contours and grayscale image at 1.4 GHz with the VLA in D configuration after subtraction of discrete sources. *Bottom, left*: total intensity radio contours of A1550 overlaid on the isodensity map of likely cluster members. *Bottom, right*: zoom of total intensity radio contours at the center of A1550 at 1.4 GHz with the VLA in C configuration. The image has a *FWHM* of $18'' \times 18''$. The first contour level is drawn at 0.15 mJy/beam, and the rest are spaced at intervals of a factor of $\sqrt{2}$. The sensitivity (1σ) is 0.04 mJy/beam. The contours of the radio intensity are overlaid on the optical image taken from the SDSS (red plate).

the RASS. In the bottom panel, the radio contours are overlaid on the isodensity map of likely cluster members. The external X-ray emission is elongated in the east-west direction, while the inner region is extended in the north-south direction. The optical galaxy distribution is bimodal but has an elongation that does not follow the cluster X-ray emission. Surrounding the X-ray and the optical center, we detected a diffuse low-surface brightness radio emission, which we classified as a radio halo. As in the case of A800, the diffuse radio emission seems to be more spatially correlated to the galaxy than to the gas over-densities.

To separate the diffuse radio emission from discrete sources, we produced an image at higher resolution. In the bottom-right panel of Fig. 3, we present the radio contours of A1550 at 1.4 GHz taken with the VLA in C configuration. This image has been convolved to a resolution of $18'' \times 18''$. The radio contours are overlaid on the optical image taken from the SDSS. Three discrete radio sources (labeled A, B, and C) are clearly embedded in the radio halo. Spots of very faint emission are also detected in the C configuration data set, but given that they do not coincide with any discrete source detected in the FIRST survey (Becker et al. 1995) we consider these emissions to be associated with the peaks of the radio halo detected in the D configuration data set.

A total flux density of $\simeq 26.5 \pm 1.3$ mJy was calculated from the D configuration image, by integrating the total intensity surface-brightness in the region of the diffuse emission down to the 3σ level. By subtracting the flux density of the discrete sources A, B, and C (see Table 2), a flux density of 7.7 ± 1.6 mJy appears to be associated with the low brightness diffuse emission. This flux density value corresponds to a radio power of $P_{1.4\,\mathrm{GHz}} = 1.49 \times 10^{24}$ W Hz^{-1}.

In the top-right panel of Fig. 3, we present the total intensity radio contours at 1.4 GHz with the VLA in D configuration after

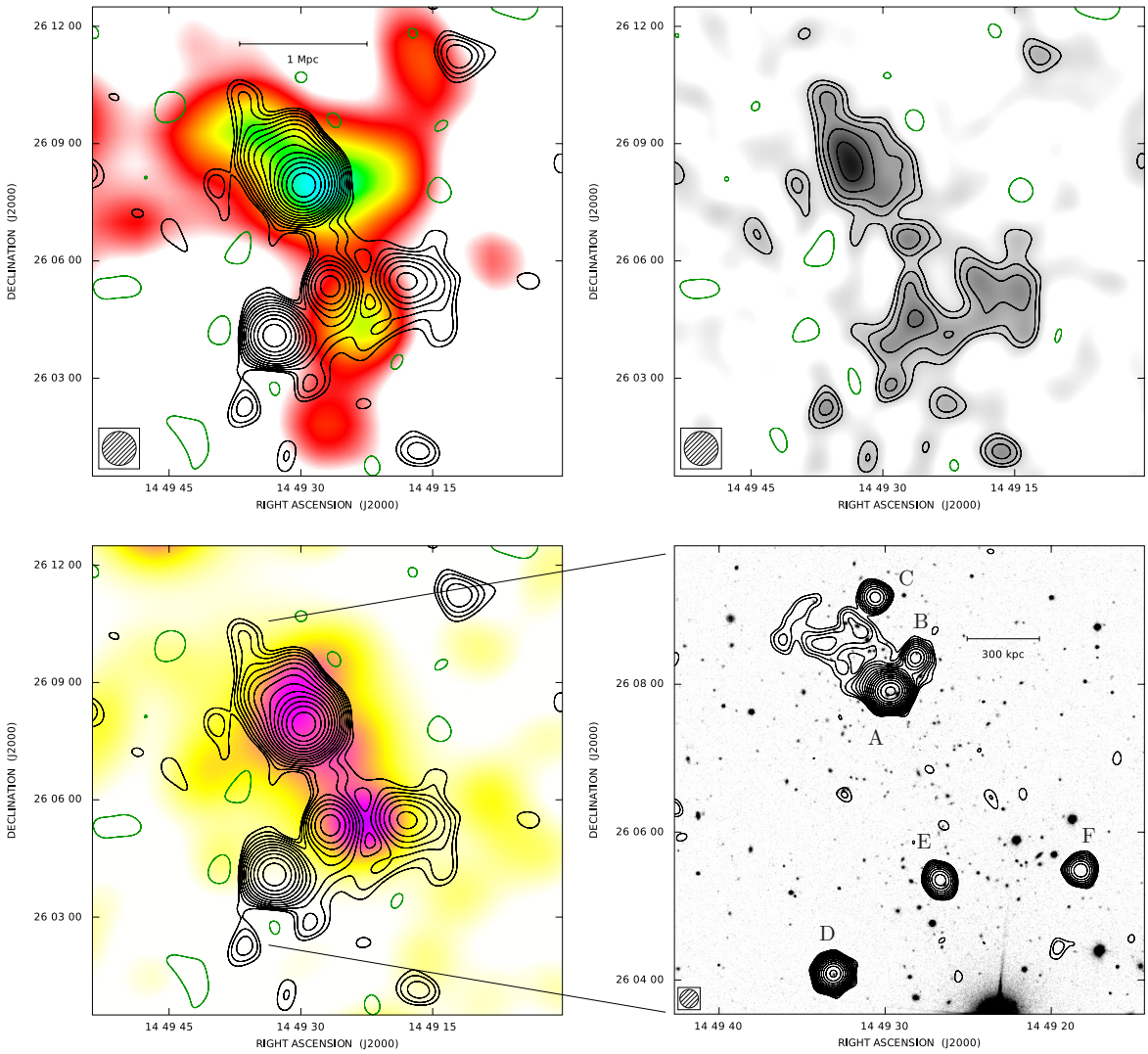

Fig. 4. CL 1446+26. *Top, left*: total intensity radio contours of CL 1446+26 at 1.4 GHz with the VLA in D configuration. The image has a *FWHM* of $52'' \times 52''$. The contour levels are drawn at -0.25, 0.25 mJy/beam, and the rest are spaced at intervals of a factor of $\sqrt{2}$. The sensitivity (1-σ) is 0.08 mJy/beam. Total intensity radio contours are overlaid on the Rosat PSPC X-ray image in the 0.1–2.4 keV band, taken from the RASS. The X-ray image has been convolved with a Gaussian of $\sigma = 45''$. *Top, right*: total intensity radio contours and grayscale image at 1.4 GHz with the VLA in D configuration after subtraction of discrete sources. *Bottom, left*: total intensity radio contours of CL 1446+26 overlaid on the isodensity map of likely cluster members. *Bottom, right*: zoom of total intensity radio contours at the center of CL1446+26 at 1.4 GHz with the VLA in C configuration, image (VLA program AO149) taken from Giovannini et al. (2009). The image has a *FWHM* of $15'' \times 15''$. The first contour level is drawn at 0.15 mJy/beam, and the rest are spaced at intervals of a factor of $\sqrt{2}$. The sensitivity (1σ) is 0.05 mJy/beam. The contours of the radio intensity are overlaid on the optical image taken from the SDSS (red plate).

subtraction of discrete sources. The flux density calculated in the image with the point sources subtracted is 8.2 ± 0.5 mJy, while as measured from the 3σ radio isophote, the radio halo shows a LLS of about $6'$ ($\simeq$1.41 Mpc).

3.4. CL 1446+26

CL 1446+26 (or CL 1447+26 or ZwCl 1447.2+2619), is a rich galaxy cluster located at $z = 0.370$ with an X-ray luminosity[3] in the 0.1−2.4 keV band of 3.41×10^{44} erg/s (Wu et al. 1999).

At radio wavelengths, it was studied by Owen et al. (1999) and Giovannini et al. (2009). The presence of a northern radio relic plus several radio galaxies were pointed out by Giovannini et al. (2009) (see also the radio contours in the bottom-right panel of Fig. 4).

Low-resolution radio contours at 1.4 GHz of CL 1446+26 are shown in the top-left and bottom-left panels of Fig. 4. This image was obtained with the VLA in D configuration and has been convolved to a resolution of $52'' \times 52''$. In the top panel, the radio contours are overlaid on the cluster X-ray image taken from the RASS. In the bottom panel, the radio contours are overlaid on the isodensity map of likely cluster members. The cluster is characterized by a disturbed morphology in both X-rays and optical, with two main clumps, one to the north and one to the south. The optical and X-ray peaks, again, are not coincident. As in A800 and A1550, the overall diffuse radio emission seems to follow more closely the galaxy than the intracluster density distribution. Our lower-resolution radio map shows the northern

[3] The bolometric X-ray luminosity has been converted to the 0.1–2.4 keV band using Table 5 of Böhringer et al. (2004), assuming an intracluster temperature of $T \simeq 5$ keV.

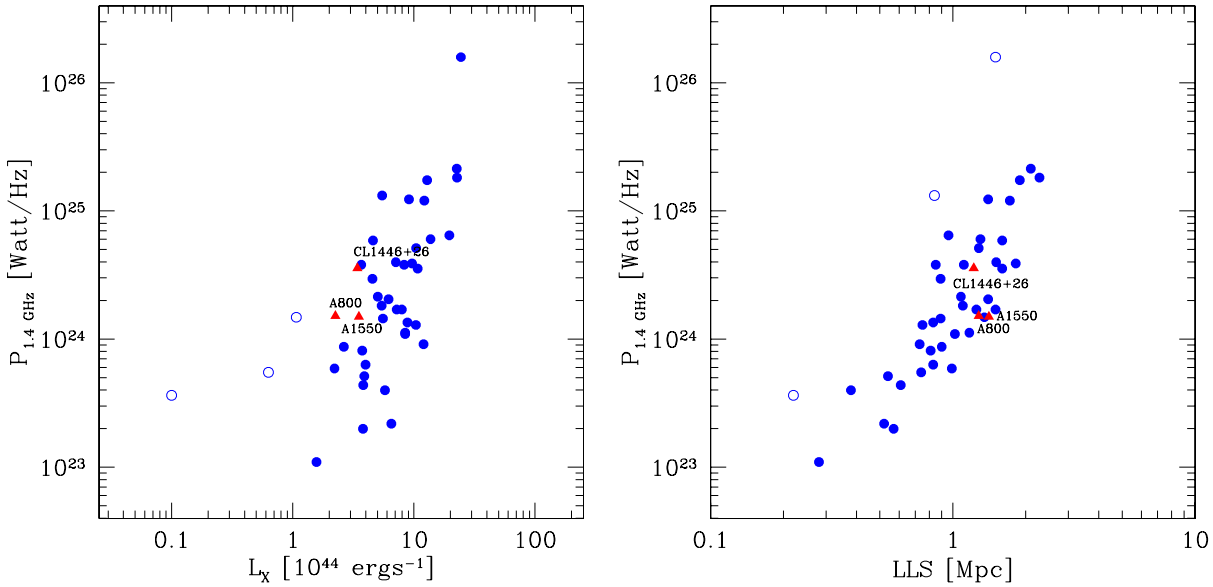

Fig. 5. *Left*: monochromatic radio power of radio halos at 1.4 GHz versus the cluster X-ray luminosity in the 0.1–2.4 keV band. *Right*: monochromatic radio power of halos at 1.4 GHz versus their LLS measured at the same frequency. The data are taken from the recent compilation of Feretti et al. (2012) and references therein. Blue dots are classical radio halos while empty blue dots are outlier clusters. The new halos detected in this work are indicated with red triangles.

clump appears to coincide with radio emission that is more extended than that obtained by Giovannini et al. (2009). In particular, this new image seems to indicate that the diffuse emission is indeed a central radio halo rather than a peripheral relic source, as previously stated. In addition, elongated diffuse radio emission in correspondence with the southern sub-cluster was newly detected.

In the top-right panel of Fig. 4, we present the total intensity radio contours at 1.4 GHz obtained with the VLA in D configuration after subtraction of discrete sources. Given their location and morphology, in the following we define the northern emission as a radio halo and the elongated southern emission as a relic. The radio halo appears to be connected through a low brightness diffuse bridge to the relic. However, a deeper follow-up observation should be made to clarify the nature of this system.

In the northern emission, a total flux density of 42.0 ± 2.1 mJy is calculated from the D configuration image, by integrating the total intensity surface-brightness in the region of the diffuse emission down to the 3σ level. By subtracting the flux density of the discrete sources A, B, and C (see Table 2) a flux density of 7.7 ± 2.6 mJy appears to be associated with the radio halo. This flux density value corresponds to a radio power of $P_{1.4\,\mathrm{GHz}} = 3.57 \times 10^{24}$ W Hz^{-1}. In the Southern emission, by subtracting the flux density of the discrete sources D, E, and F from the total flux density (22.0 ± 1.1 mJy), a flux density of 5.3 ± 1.2 mJy appears to be associated with the relic. This flux density value corresponds to a radio power of $P_{1.4\,\mathrm{GHz}} = 2.46 \times 10^{24}$ W Hz^{-1}. The LLS is about $4'$ ($\simeq$1.22 Mpc) and $5'$ ($\simeq$1.53 Mpc) for the radio halo and relic, respectively. The flux densities calculated in the image with the point sources subtracted are consistent within the errors with the values given in Table 3, being 5.3 ± 0.3 mJy in the halo and 5.5 ± 0.3 mJy in the relic.

4. Statistical properties

The basic properties of the new diffuse cluster radio sources (halos and relics) are reported in Table 3. The new relics presented here have similar properties to other published relic sources (see e.g. the statistical characteristics of radio relics reviewed by Feretti et al. 2012), and are not discussed further in the following.

All the clusters presented in this paper that host new radio halos (A800, A1550, CL1446+26) display a clear shift between the galaxies and gas distribution, as well as complex optical and X-ray morphologies. Joint numerical and observational analyses indicate that these are typical features of dynamically disturbed clusters that have had or are undergoing a major merging event (e.g. Maurogordato et al. 2011). Deeper X-ray observations and optical spectroscopic follow-up could help in re-constructing the collision scenario of these perturbed systems.

In Fig. 5, we plot the radio power calculated at 1.4 GHz ($P_{1.4\ \mathrm{GHz}}$) versus both the cluster X-ray luminosity in the 0.1–2.4 keV band (L_X) and the *LLS*. The blue dots refer to radio halos taken from the literature. Among them, the empty dots are outliers, i.e. in the left panel they refer to the few known radio halos A523 (Giovannini et al. 2011), A1213 (Giovannini et al. 2009), and 0217+70 (Brown et al. 2011) that are over-luminous in radio with respect to the cluster X-ray luminosity, while in the right panel they refer to the few known radio halos A1213, A1351 (Giovannini et al. 2009), and MACS J0717.5+3745 (Bonafede et al. 2009), which shows a size smaller than expected from their radio power. The new radio halos are indicated with red triangles. They agree with both the $P_{1.4\ \mathrm{GHz}} - L_X$ and $P_{1.4\ \mathrm{GHz}} - LLS$ relations known for the other halos in clusters.

The observed correlation between the radio power of halos and their size was firstly discovered for giant radio halos by Cassano et al. (2007). In a later analysis, Murgia et al. (2009) by fitting the azimuthally averaged brightness profile with an exponential found that the radio halo emissivity is remarkably similar from one halo to the other, despite the quite different length-scales, in agreement with the $P_{1.4\ \mathrm{GHz}} - LLS$ correlation where larger halos have a higher radio power.

A close similarity between the radio and the X-ray structures has been found in a number of clusters hosting a radio halo (see e.g. Govoni et al. 2001b). This similarity is generally valid for

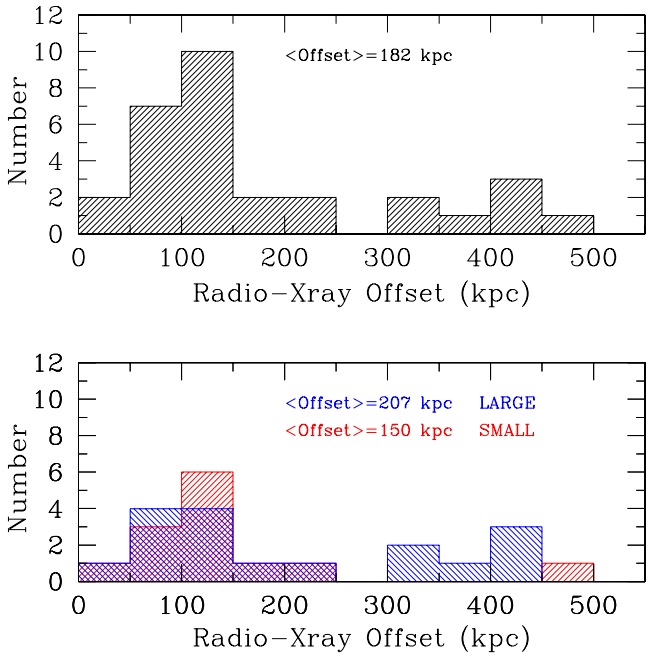

Fig. 6. *Top*: offset between the radio and X-ray peaks for a sample of radio halos (see Table 4). *Bottom*: offset between the radio and X-ray peaks. The blue dashed area refers to giant halos (*LLS* > 1 Mpc) and the red dashed area refers to small halos (*LLS* < 1 Mpc), respectively.

giant and regular halos. However, more irregular and asymmetric halos have been found in the literature. In these halos, the radio emission may show significant displacement from the X-ray emission. Interestingly, the new halos studied in this paper display a clear offset between the radio and the X-ray peaks (see Table 3). In addition, the similarity between the radio and the X-ray morphologies is not clearly present and the radio emission seems to more closely follow the galaxy distribution than the intracluster gas-density distribution.

To investigate from a statistical point of view the offset between the radio halo and the X-ray peak of the cluster emission, we followed the analysis of Feretti et al. (2011).

In the top panel of Fig. 6, we present the distribution of the offset between the peak position of the radio halo and the X-ray gas distribution for the new radio halos presented in this paper together with a sample of clusters at redshifts $z \leq 0.4$ previously imaged at 1.4 GHz by our group (following a uniform data-reduction strategy), for which good radio and X-ray data are available (see Table 4 for details). The mean radio-X-ray offset is 182 kpc. In the bottom panel of Fig. 6, the same distribution refers to large halos with *LLS* > 1 Mpc (in blue) and small halos with *LLS* < 1 Mpc (in red), respectively. Both large and small radio halos appear to be significantly shifted, by up to hundreds kpc, with respect to the X-ray center.

To highlight radio halos with the most pronounced asymmetric distribution, the radio-X-ray offset normalized to the halo size (*LLS*) is plotted in Fig. 7. The mean value of the radio-X-ray offset normalized to the *LLS* is 0.19. In the bottom panel of Fig. 7, the same distribution is considered separately for large (in blue) and small (in red) halos. The mean value calculated for large halos is 0.15, while the mean value calculated for small halos is 0.24. Thus, we found that halos can be quite asymmetric with respect to the X-ray gas distribution, and this becomes more relevant when halos of smaller size are considered.

Table 4. Radio-X-ray offsets for a sample of halos.

Name	z	kpc/″	Radio-X-ray offset (″)	LLS (′)	Ref.
A209	0.2060	3.34	20	7.0	1
A399	0.0718	1.35	135	7.0	2
A401	0.0737	1.38	70	6.3	3
A520	0.1990	3.25	20	5.7	4
A523	0.1036	1.88	185	12.0	5
A545	0.1540	2.64	50	5.6	3
A665	0.1819	3.03	50	10	6
A754	0.0542	1.04	142	15.8	3
A773	0.2170	3.48	30	6.0	4
A781	0.3004	4.42	55	6.0	7
A800	0.2223	3.55	90	6.0	*
A851	0.4069	5.40	75	3.3	1
A1213	0.0469	0.91	145	4.0	1
A1351	0.3224	4.65	100	3.0	1
A1550	0.2540	3.92	105	6.0	*
A1689	0.1832	3.05	15	4.0	8
A1758a	0.2790	4.20	35	6.0	1
A1914	0.1712	2.88	45	7.4	3
A1995	0.3186	4.61	45	3.0	1
A2034	0.1130	2.03	65	5.0	1
A2163	0.2030	3.31	30	11.5	9
A2218	0.1756	2.94	35	2.2	10
A2219	0.2256	3.59	20	8.0	3
A2254	0.1780	2.98	45	5.0	4
A2255	0.0806	1.50	65	10.0	11
A2294	0.1780	2.98	25	3.0	1
A2319	0.0557	1.07	35	15.9	12
A2744	0.3080	4.50	25	7.0	4
RXCJ1314	0.2439	3.81	100	7.0	13
CL1446+26	0.3700	5.09	85	4.0	*

Notes. Column 1: cluster name; Col. 2: redshift; Col. 3: angular-to-linear conversion; Col. 4: radio - X-ray offset; Col. 5: radio LLS; Col. 6: reference to the radio halos at 1.4 GHz: * = this work, 1 = Giovannini et al. (2009), 2 = Murgia et al. (2010), 3 = Bacchi et al. (2003), 4 = Govoni et al. (2001a), 5 = Giovannini et al. (2011), 6 = Vacca et al. (2010), 7 = Govoni et al. (2011), 8 = Vacca et al. (2011), 9 = Feretti et al. (2001), 10 = Giovannini & Feretti (2000), 11 = Govoni et al. (2005), 12 = Feretti et al. (1997), 13 = Feretti et al. (2005).

5. Discussion

Although the properties of the newly discovered, moderate-mass, radio halos are consistent with the $P_{1.4\,\mathrm{GHz}} - L_X$ and $P_{1.4\,\mathrm{GHz}} - LLS$ correlations known in the literature, their radio morphology does not exactly matches the thermal X-ray emission from the intracluster medium.

By analyzing the radio X-ray offset statistically, we found a tendency for smaller halos to show larger displacements. This result may have important consequences for the origin of radio halos, suggesting that the morphological properties of radio halos may be linked to the cluster dynamical state.

Major cluster mergers can supply energy to the radio-emitting particles, as well as amplify magnetic fields (e.g. Roettiger et al. 1999; Dolag et al. 1999; Ricker & Sarazin 2001; Dolag et al. 2005; Ryu et al. 2008; Vazza et al. 2009; Xu et al. 2010; Vazza et al. 2011; Xu et al. 2011). Since magnetic fields have been found to be ubiquitous in galaxy clusters (e.g. Kronberg 1994; Carilli & Taylor 2002; Clarke et al. 2001; Govoni & Feretti 2004; Bonafede et al. 2011), the crucial ingredient for the existence of diffuse radio halos is the presence of synchrotron electrons with GeV energies. The continuous

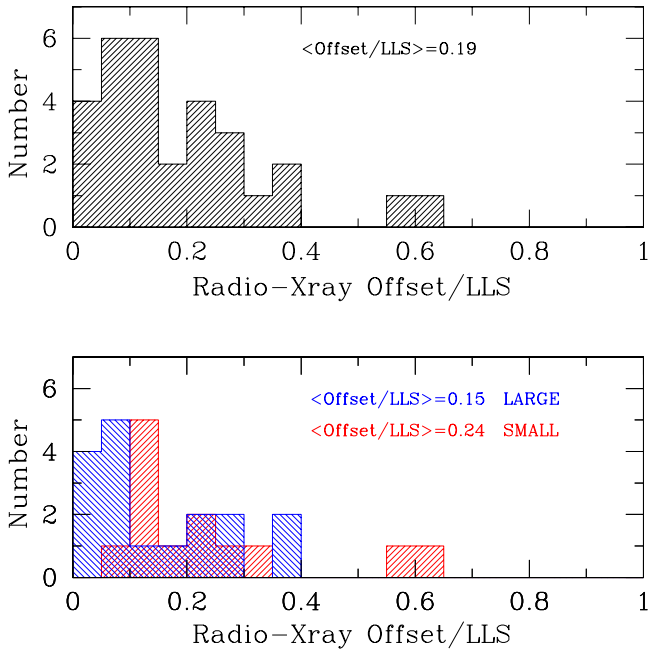

Fig. 7. *Top*: fractional offset (Offset/*LLS*) between the radio and X-ray peaks for a sample of radio halos (see Table 4). *Bottom*: fractional offset (Offset/*LLS*) between the radio and X-ray peaks. The blue dashed area refers to giant halos (*LLS* > 1 Mpc) and the red dashed area refers to small halos (*LLS* < 1 Mpc), respectively.

acceleration of thermal electrons in galaxy clusters is actually impossible because the energy gained by the particles is dissipated to the whole plasma on a timescale much shorter than that of the acceleration process itself (see e.g. Petrosian 2001; Wolfe & Melia 2006). On the other hand, it is believed that primary relativistic electrons are present in the cluster volume because they have been injected by either active galactic nucleus activity or star-forming galaxies during the cluster dynamical history. This population of electrons suffers strong radiation losses mainly because of synchrotron and inverse Compton emission, thus direct or stochastic re-acceleration caused by merging shocks and turbulence is needed to maintain their energy to the level necessary to produce the observed synchrotron radio emission in the relatively weak intracluster magnetic fields (e.g. Jaffe 1977; Schlickeiser et al. 1987; Petrosian 2001; Brunetti et al. 2001; Brunetti et al. 2011). Alternatively, electrons can be continuously injected into the intracluster medium as secondary particles by inelastic nuclear collisions between relativistic protons and nuclei in the thermal ambient intracluster medium (e.g. Dennison 1980; Kushnir et al. 2009; Keshet & Loeb 2010; Enßlin et al. 2011). The protons diffuse on large scales because their energy losses are negligible. They can continuously produce in situ electrons, distributed throughout the cluster volume. The possibility that the high energy electrons responsible for the synchrotron emission arise from the decay of secondary products of the neutralino annihilation in the dark matter halos of galaxy clusters has also been suggested (Colafrancesco & Mele 2001).

A detailed discussion of the origin of the non-thermal emission in galaxy clusters was beyond the aims of this work, which were in fact mainly observational. Nevertheless, we can explore, from a qualitative perspective, the reasons for the larger distortions and offsets observed among the smallest halos. Cluster merger events are expected to release a significant amount of energy into the intracluster medium. This energy is injected on large spatial scales, and then turbulent cascades may be generated. It is generally believed that a fraction of this energy is finally channeled into relativistic particles acceleration and magnetic field amplification. Thus, in this framework, the observed offsets could be related to the age of the merger.

A possible explanation of this behavior is the presence of intracluster magnetic field spatial variations on large scales and/or a non-uniform distribution of relativistic electrons. On the basis of modeling, Vacca et al. (2010) found that if the intracluster magnetic field and relativistic electrons fluctuations are close to the observing beam scale, the halo results smooth and rounded. Increasing the magnetic field and the relativistic electrons correlation length results in a much more distorted radio halo morphology and a significant offset of the radio halo peak from the cluster center. Therefore, smaller halos may have a more distorted morphology because they may be young systems in which there is still energy on large scales, leading to a non-uniform distribution of relativistic electrons and/or a magnetic field correlation length larger than in the more extended, and dynamical older, radio halos.

6. Conclusions

To investigate the presence of extended, diffuse radio sources in galaxy clusters, we have studied the radio continuum emission in a sample of galaxy clusters by analyzing archival VLA observations at 1.4 GHz in D configuration. These observations have been complemented by X-ray, optical, and higher-resolution radio data. The higher-resolution radio images help us to confirm that the detected diffuse emission is real and not due to a blend of discrete sources. The point source subtraction is rather relevant for the detection of diffuse radio emission and the associated flux density. Therefore, this procedure has been performed carefully using different methods.

These data permitted us to increase the number of detections of large-scale, diffuse, radio emission. We discovered a new radio halo in the central regions of A800 and A1550. We detected a radio relic in the periphery of A910. Finally, we revealed both a halo and a relic in CL1446+26.

All the clusters presented in this paper hosting new radio halos display a clear shift between the galaxies and gas distribution as well as complex optical and X-ray morphologies, which are typical features of dynamically disturbed clusters. The radio X-ray similarity is not clearly present and the radio emission seems to more closely follow the galaxy distribution than the intracluster gas distribution. Interestingly, there is a clear offset between the radio and the X-ray peaks.

By analyzing this offset statistically, we found that radio halos can be quite asymmetric with respect to the X-ray gas distribution, particularly when we considered halos of smaller size. This behavior could be linked to the cluster dynamical state. Vacca et al. (2010) found that a very distorted radio halo morphology and a significant offset of the radio halo peak from the cluster center is expected increasing the magnetic field and the relativistic electrons correlation length in galaxy clusters. Therefore, smaller halos may have more distorted morphologies because they may be young systems in which the merger energy is still on large scales, leading to a non-uniform distribution of relativistic electrons and/or a magnetic field correlation length larger than in the more extended, and dynamical older, radio halos. Thus, in this framework, the observed offsets could be related to the age of the merger.

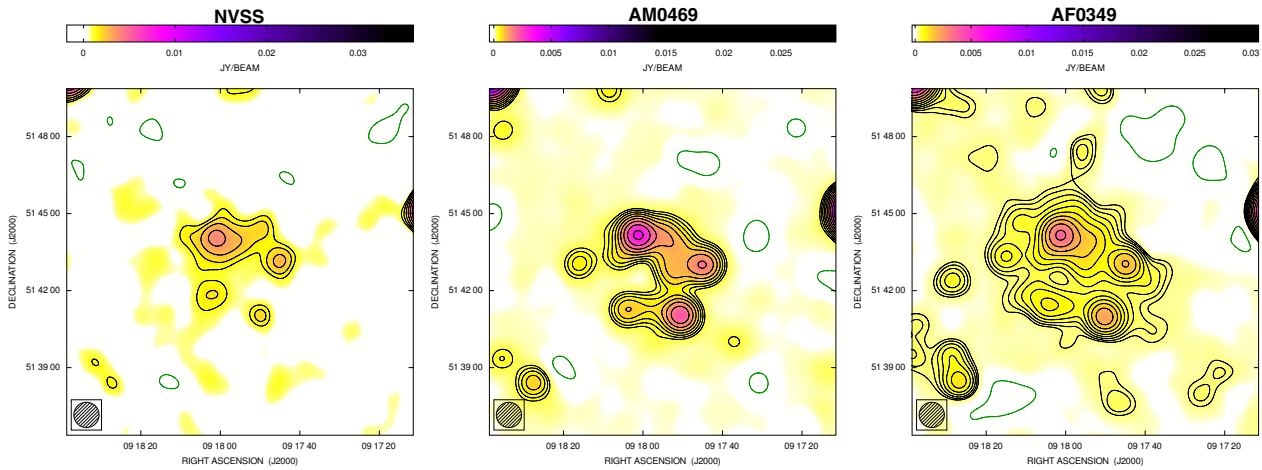

Fig. A.1. Total intensity radio contours of A773 at 1.4 GHz obtained with different VLA data sets. All images have been convolved to a FWHM resolution of $59'' \times 59''$. *Left*: image from the NVSS (Condon et al. 1998). The contour levels are drawn at -1.2 (green), $+1.2$ mJy/beam, and the rest are spaced at intervals of a factor of $\sqrt{2}$. *Middle*: image obtained from the AM0469 data set. The contour levels are drawn at -0.2 (green), $+0.2$ mJy/beam, and the rest are spaced at intervals of a factor of $\sqrt{2}$. *Right*: image obtained from the AF0469 data set (Govoni et al. 2001a). The contour levels are drawn at -0.15 (green), $+0.15$ mJy/beam, and the rest are spaced at intervals of a factor of $\sqrt{2}$.

Acknowledgements. We thank the referee for suggestions that improved the presentation of the paper. This research was partially supported by PRIN-INAF2009. We acknowledge financial contribution from the agreement ASI-INAF I/009/10/0. C.F. and C.B. acknowledge financial support by the "*Agence Nationale de la Recherche*" through grant ANR-09-JCJC-0001-01. The National Radio Astronomy Observatory (NRAO) is a facility of the National Science Foundation, operated under cooperative agreement by Associated Universities, Inc. Funding for the SDSS and SDSS-II has been provided by the Alfred P. Sloan Foundation, the Participating Institutions, the National Science Foundation, the US Department of Energy, the National Aeronautics and Space Administration, the Japanese Monbukagakusho, the Max Planck Society, and the Higher Education Funding Council for England. The SDSS Web Site is http://www.sdss.org/. This research made use of Montage, funded by the National Aeronautics and Space Administration's Earth Science Technology Office, Computational Technnologies Project, under Cooperative Agreement Number NCC5-626 between NASA and the California Institute of Technology. The code is maintained by the NASA/IPAC Infrared Science Archive.

Appendix A: Images reliability

In this work we made use of the archival VLA data set AM0469 to collect evidence of diffuse radio emission in galaxy clusters. AM0469 contains about 40 clusters. Some of them, like A773, were already known to host a radio halo. To compare the quality of this data set with other observations, in Fig. A.1 we present the A773 field of view as seen with the NRAO VLA Sky Survey (NVSS; Condon et al. 1998), the AM0469 data set, and a deeper ($\simeq$4 h) VLA observation in C and D configurations (Govoni et al. 2001a, VLA program AF0349). For a proper comparison images have been smoothed to a common resolution of $59'' \times 59''$. We note that in the AM0469 data set we missed some diffuse cluster emission, that is instead revealed in the deeper observation. However, this data set is fairly sensitive than the NVSS. We remark that a significant breakthrough in the study of radio halos was obtained thanks to the NVSS (Giovannini et al. 1999).

References

Abazajian, K. N., Adelman-McCarthy, J. K., Agüeros, M. A., et al. 2009, ApJS, 182, 543
Bacchi, M., Feretti, L., Giovannini, G., & Govoni, F. 2003, A&A, 400, 465
Basu, K. 2012, MNRAS, 421, L112
Becker, R. H., White, R. L., & Helfand, D. J. 1995, ApJ, 450, 559
Böhringer, H., Voges, W., Huchra, J. P., et al. 2000, ApJS, 129, 435
Böhringer, H., Schuecker, P., Guzzo, L., et al. 2004, A&A, 425, 367
Bonafede, A., Feretti, L., Giovannini, G., et al. 2009, A&A, 503, 707
Bonafede, A., Govoni, F., Feretti, L., et al. 2011, A&A, 530, A24
Brown, S., & Rudnick, L. 2011, MNRAS, 412, 2
Brown, S., Duesterhoeft, J., & Rudnick, L. 2011, ApJ, 727, L25
Brunetti, G. 2011, Mem. Soc. Astron. Italiana, 82, 515
Brunetti, G., Setti, G., Feretti, L., & Giovannini, G. 2001, MNRAS, 320, 365
Buote, D. A. 2001, ApJ, 553, L15
Carilli, C. L., & Taylor, G. B. 2002, ARA&A 40, 319
Cassano, R., Brunetti, G., Setti, G., Govoni, F., & Dolag, K. 2007, MNRAS, 378, 1565
Cassano, R., Ettori, S., Giacintucci, S., et al. 2010, ApJ, 721, L82
Clarke, T. E., Kronberg, P. P., & Böhringer, H. 2001, ApJ, 547, L111
Colafrancesco, S. 1999, Diffuse Thermal and Relativistic Plasma in Galaxy Clusters, 269
Colafrancesco, S., & Mele, B. 2001, ApJ, 562, 24
Condon, J. J., Cotton, W. D., Greisen, E. W., et al. 1998, AJ 115, 1693
Dennison, B. 1980, ApJ, 239, L93
Dolag, K., Bartelmann, M., & Lesch, H. 1999, A&A, 348, 351
Dolag, K., Vazza, F., Brunetti, G., & Tormen, G. 2005, MNRAS, 364, 753
Ebeling, H., Edge, A. C., Allen, S. W., et al. 2000, MNRAS, 318, 333
Enßlin, T., Pfrommer, C., Miniati, F., & Subramanian, K. 2011, A&A, 527, A99
Feretti, L. 2002, The Universe at Low Radio Frequencies, IAU Sump., 199, 133
Feretti, L., Giovannini, G., & Bohringer, H. 1997, New Astron., 2, 501
Feretti, L., Fusco-Femiano, R., Giovannini, G., & Govoni, F. 2001, A&A, 373, 106
Feretti, L., Schuecker, P., Böhringer, H., Govoni, F., & Giovannini, G. 2005, A&A, 444, 157
Feretti, L., Giovannini, G., Govoni, F., & Murgia, M. 2011, IAU Symp., 274, 340
Feretti, L., Giovannini, G., Govoni, F., & Murgia, M. 2012, A&ARv, 20, 54
Ferrari, C., Benoist, C., Maurogordato, S., Cappi, A., & Slezak, E. 2005, A&A, 430, 19
Ferrari, C., Govoni, F., Schindler, S., Bykov, A. M., & Rephaeli, Y. 2008, Space Sci. Rev., 134, 93
Giacintucci, S., Venturi, T., Cassano, R., et al. 2009, ApJ, 704, L54
Giovannini, G., & Feretti, L. 2000, New Astron., 5, 335
Giovannini, G., Tordi, M., & Feretti, L. 1999, New A, 4, 141
Giovannini, G., Bonafede, A., Feretti, L., et al. 2009, A&A, 507, 1257
Giovannini, G., Feretti, L., Girardi, M., et al. 2011, A&A, 530, L5
Goto, T., Sekiguchi, M., Nichol, R. C., et al. 2002, AJ, 123, 1807
Govoni, F., & Feretti, L. 2004, Int. J. Mod. Phys. D, 13, 1549
Govoni, F., Feretti, L., Giovannini, G., et al. 2001a, A&A, 376, 803
Govoni, F., Enßlin, T. A., Feretti, L., & Giovannini, G. 2001b, A&A, 369, 441
Govoni, F., Markevitch, M., Vikhlinin, A., et al. 2004, ApJ, 605, 695
Govoni, F., Murgia, M., Feretti, L., et al. 2005, A&A, 430, L5
Govoni, F., Murgia, M., Feretti, L., et al. 2006, A&A, 460, 425
Govoni, F., Murgia, M., Giovannini, G., Vacca, V., & Bonafede, A. 2011, A&A, 529, A69

Greisen, E. W., Spekkens, K., & van Moorsel, G. A. 2009, AJ, 137, 4718
Hambly, N. C., MacGillivray, H. T., Read, M. A., et al. 2001, MNRAS, 326, 1279
Jaffe, W. J. 1977, ApJ, 212, 1
Kempner, J. C., & Sarazin, C. L. 2001, ApJ, 548, 639
Keshet, U., & Loeb, A. 2010, ApJ, 722, 737
Kronberg, P. P. 1994, Rep. Progr. Phys., 57, 325
Kushnir, D., Katz, B., & Waxman, E. 2009, Cosmol. Astropart. Phys., 9, 24
Liang, H. 1999, Diffuse Thermal and Relativistic Plasma in Galaxy Clusters, MPE Report, 271, 33
Maurogordato, S., Sauvageot, J. L., Bourdin, H., et al. 2011, A&A, 525, 79
Murgia, M., Govoni, F., Feretti, L., et al. 2004, A&A, 424, 429
Murgia, M., Govoni, F., Markevitch, M., et al. 2009, A&A, 499, 679
Murgia, M., Govoni, F., Feretti, L., & Giovannini, G. 2010, A&A, 509, A86
Orrú, E., Murgia, M., Feretti, L., et al. 2007, A&A, 467, 943
Owen, F., Morrison, G., & Voges, W. 1999, Diffuse Thermal and Relativistic Plasma in Galaxy Clusters, MPE Report, 271, 9
Petrosian, V. 2001, ApJ, 557, 560
Pizzo, R. F., de Bruyn, A. G., Bernardi, G., & Brentjens, M. A. 2011, A&A, 525, A104
Ricker, P. M., & Sarazin, C. L. 2001, ApJ, 561, 621
Roettiger, K., Stone, J. M., & Burns, J. O. 1999, ApJ, 518, 594
Rossetti, M., Eckert, D., Cavalleri, B. M., et al. 2011, A&A, 532, A123
Rudnick, L., & Lemmerman, J. A. 2009, ApJ, 697, 1341
Ryu, D., Kang, H., Cho, J., & Das, S. 2008, Science, 320, 909
Schlickeiser, R., Sievers, A., & Thiemann, H. 1987, A&A, 182, 21
Schuecker, P., Böhringer, H., Reiprich, T. H., & Feretti, L. 2001, A&A, 378, 408
Tribble, P. C. 1991, MNRAS, 253, 147
van Weeren, R. J., Röttgering, H. J. A., Brüggen, M., & Cohen, A. 2009, A&A, 508, 75
van Weeren, R. J., Brüggen, M., Röttgering, H. J. A., et al. 2011, A&A, 533, A35
Vacca, V., Murgia, M., Govoni, F., et al. 2010, A&A, 514, A71
Vazza, F., Brunetti, G., Kritsuk, A., et al. 2009, A&A, 504, 33
Vazza, F., Brunetti, G., Gheller, C., Brunino, R., & Brüggen, M. 2011, A&A, 529, A17
Venturi, T., Giacintucci, S., Brunetti, G., et al. 2007, A&A, 463, 937
Venturi, T., Giacintucci, S., Dallacasa, D., et al. 2008, A&A, 484, 327
Xu, H., Li, H., Collins, D. C., Li, S., & Norman, M. L. 2010, ApJ, 725, 2152
Xu, H., Li, H., Collins, D. C., Li, S., & Norman, M. L. 2011, ApJ, 739, 77
Wolfe, B., & Melia, F. 2006, ApJ, 638, 125
Wu, X.-P., Xue, Y.-J., & Fang, L.-Z. 1999, ApJ, 524, 22